
Article:
Parry, J.A., Horoshenkov, K.V. orcid.org/0000-0002-6188-0369 and Williams, D.P. (2020) Investigating uncertain geometries effect on sound propagation in a homogeneous and non-moving atmosphere over an impedance ground. Applied Acoustics, 160. ISSN: 0003-682X

https://doi.org/10.1016/j.apacoust.2019.107122

Investigating Uncertain Geometries Effect on Sound Propagation in a Homogeneous and Non-moving Atmosphere Over an Impedance Ground

Jordan A. Parry[1], Kirill V. Horoshenkov[1], Duncan P. Williams[2]
[1]University of Sheffield, Department of Mechanical Engineering, Sheffield, England
JAParry1@Sheffield.ac.uk; K.Horoshenkov@Sheffield.ac.uk
[2]Defence Science and Technology Laboratory (DSTL), Salisbury, England
DPWilliams@dstl.gov.uk

Abstract

Predicting outdoor sound in uncertain conditions is a difficult task and there are limited data which enable us to relate accurately the variations in the conditions in the propagation path with the fluctuations in the received acoustical signal. This paper investigates, though numerical simulations, the effect of uncertainties on sound propagation in a homogeneous atmosphere over an impedance ground. A simple Monte Carlo method is used to understand the effect of uncertainties in the source and receiver positions on the excess attenuation. The ratio of source/receiver height to the horizontal source/receiver separation is found to influence strongly the statistical distribution of the resultant excess attenuation spectrum. Impedance ground and level of uncertainty are found to be influential only for specific statistics while all samples were found to violate normality. These findings help to increase understanding of the role of uncertainties in outdoor sound propagation, accuracy of source characterization based on parameter inversion and at lower computational costs.

Keywords

Outdoor sound propagation; Uncertainty; Impedance ground; Receiver geometry;
Homogeneous atmosphere; Probability density function.

1 Introduction

Predicting outdoor sound is a complex problem particularly when there an uncertainty in the parameters involved. Comprehensive quantification of uncertainties in relation to outdoor acoustics remains challenging. One recent paper related to uncertainties in outdoor sound propagation concluded that uncertainties within the characteristics of the ground and atmosphere dominate uncertainties in the predicted sound pressure[1]. A subsequent paper by the same research team found that the impact of uncertainty from the range and source height were equal and that the temperature gradient was only influential at short ranges and at high frequencies[2]. Sound levels were found to be more accurately predicted in downwind situations comparted to upwind. The authors also highlighted the importance balancing the trade-off point between model complexity & computational effort.

The above work points out to the difficulties in isolating specific effects leading to outdoor sound measurement uncertainties and complexity of the interactions between key parameters many of which are not known. Complex models used in the case of inhomogeneous settings (e.g. atmospheric effects) can have better predication accuracy provided the values of the input parameters are accurately known[3]. However, there is a lack of data on the sensitivity of these models to some uncertainty in the input parameter values. In this respect, moving back to simpler models allows for a clearer understanding of the statistics which describe the uncertainties in predictions for sound propagation in homogenous, and non-moving, atmosphere but with uncertain source position and ground conditions. Simpler models are able to accurately predict impedance of the ground and isolate this effect form the uncertainty in the source geometry.

Prediction of the ground effect on outdoor sound pressure from a point source at a known position is a reasonably routine matter. A considerable amount of work has been done to study this effect. Harriot and Hothersall investigated propagation, using multiple methods, over an impedance ground in an infinite plane, in

a non-moving homogenous atmosphere, while computational costs were also considered[4]. The specific geometry where source-receiver heights where 1 – 4 m across 50 m range at 1 kHz frequency created strong destructive interference between the direct and reflected waves. Accuracy in results was found to be highest for combinations of greater source-receiver heights or shorter source-receive distances. More expansive methods were later applied by Kruse and Mellert[5]. They used a two-microphone method to measure errors due to an impedance ground under also under the assumption of a non-moving homogenous atmosphere. For low impedance surfaces, acceptable accuracy was found at frequencies above 100 Hz, while higher flow resistivity grounds shown use of the predefined geometries may not be recommended for frequencies below 500 Hz. Although the results in ref. [5] relate directly to the problem of sound propagation in the presence of an impedance ground, this work does not present any statistical data that can be used to characterise the uncertainty in the excess attenuation, especially in the case of large variability in the source position.

In general, the effects of uncertainty in key model parameters on prediction of outdoor sound propagation and acoustic source characterisation are greatly understudied. This becomes the motivation for our study with the primary question of this paper: *How does an uncertainty in geometrical parameters affect the broadband excess attenuation of sound for a relatively simple source-receiver geometry?* The excess attenuation is an important parameter which is routinely used to predict the influence of the ground, topography and meteorological conditions on sound pressure level at the receiver position[3]. Removal of other complexities to understand the effects will build stronger foundations to progress further developments for more complex research and application. Therefore, understanding of the effect of uncertainties on this parameter is of importance to several applications, which include environmental noise control, source characterisation and environmental monitoring.

The purpose of this paper is to study the effect of uncertainty in the range and source height on the statistical properties of the excess attenuation spectrum for a range of ground conditions. We structure the paper in the following manner. Section 2.1 details the acoustical model and ground effect, section 2.2 details the statistical simulation setup, and section 3 reviews the results from this simulation. Finally, section 4 is our conclusions.

2 Research Methods

2.1 Model Development

2.1.1 Initial Acoustic Model

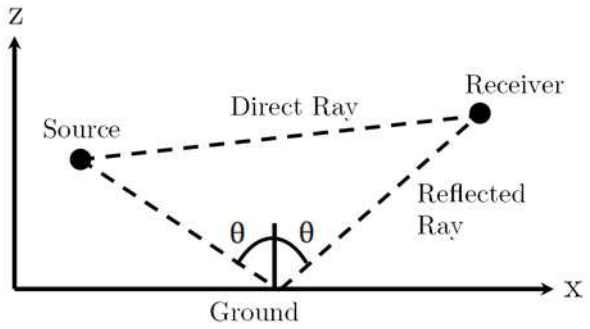

Figure 1: Diagram of acoustical scenario with impedance ground and incident angle highlighted.

Let us assume that a sound wave radiated by a point source propagates above a porous ground in a homogeneous atmosphere. This means that the effects of atmospheric parameters such as wind and temperature gradients can be excluded, leaving only the geometrical parameters such as the source and receiver height and their horizontal separation. This geometric scenario is illustrated in Figure 1. We assume that the problem is symmetrical, i.e. the sound pressure is predicted in an (x,z) co-ordinate system and the source and receiver are located at $(0,z_s)$ and (r,z), respectively. The complex sound pressure at the receiver position is[3]

$$p_c = p_{free}\left[1 + Q\frac{R_1}{R_2}\exp\left(ikR_2 - ikR_1\right)\right], \#(\mathbf{1})$$

with

$$R_1 = \sqrt{r^2 + (z - z_s)^2}\ ,\#(\mathbf{2})$$

$$R_2 = \sqrt{r^2 + (z + z_s)^2}\ .\#(\mathbf{3})$$

k and Q are the wavenumber and spherical wave reflection co-efficient, respectively. p_{free} is the sound pressure in the absence of the impedance ground. The imaginary part of the wavenumber accounts for the attenuation in air. The reflection coefficient accounts for the proportion of the incident sound pressure reflected from the porous ground and any phase changes the reflected acoustic wave undergoes due to the ground effect. As detailed by Salomons in his book[6], the equation for the spherical wave reflection coefficient is

$$Q = \left(\frac{Z\cos\theta - 1}{Z\cos\theta + 1}\right) + \left(1 - \left(\frac{Z\cos\theta - 1}{Z\cos\theta + 1}\right)\right)F(w)\ .\#(\mathbf{4})$$

The angle θ is the incident angle as shown in Figure 1. The function $F(w)$ is the boundary loss factor

$$F(w) = 1 + iw\sqrt{\pi}\exp(-w)\mathrm{erfc}(-iw)\ ,\#(\mathbf{5})$$

and $\mathrm{erfc}(-iw)$ the complimentary error function

$$\mathrm{erfc}(z) = \frac{1}{\sqrt{2\pi}}\int_z^\infty \exp(-t^2)dt\ .\#(\mathbf{6})$$

The parameter Z seen in eq. (4) is the normalised impedance of the ground, which depends greatly on the ground characteristics. The sound pressure levels in the presence and absence of the ground are

$$p_c \rightarrow L_p = 10\log_{10}\left(\frac{|p_c|^2}{2p_{ref}^2}\right),\ \#(\mathbf{7})$$

$$p_{free} \rightarrow L_{p,free} = 10\log_{10}\left(\frac{|p_{free}|^2}{2p_{ref}^2}\right),\#(\mathbf{8})$$

respectively. Combining eq. (7) and eq. (8) gives

$$L_p = L_{p,\,free} + \Delta L\ .\#(\mathbf{9})$$

The term ΔL in eq. (9) is the relative sound pressure level, or excess attenuation. This term can be expressed as

$$\Delta L = 10\log_{10}\left|1 + Q\frac{R_1}{R_2}\exp(ikR_2 - ikR_1)\right|^2\ .\#(\mathbf{10})$$

This value physically represents deviation from the free field due to the influence of the ground. The excess attenuation can take positive and negative values that correspond to the constructive and destructive interference between the direct and reflected waves, respectively. The excess attenuation is used for a wide range of acoustics purposes, especially in outdoor acoustics, which is why it will be the predicted value in question during the analysis of the influence of the parameter uncertainties. Examples of possible

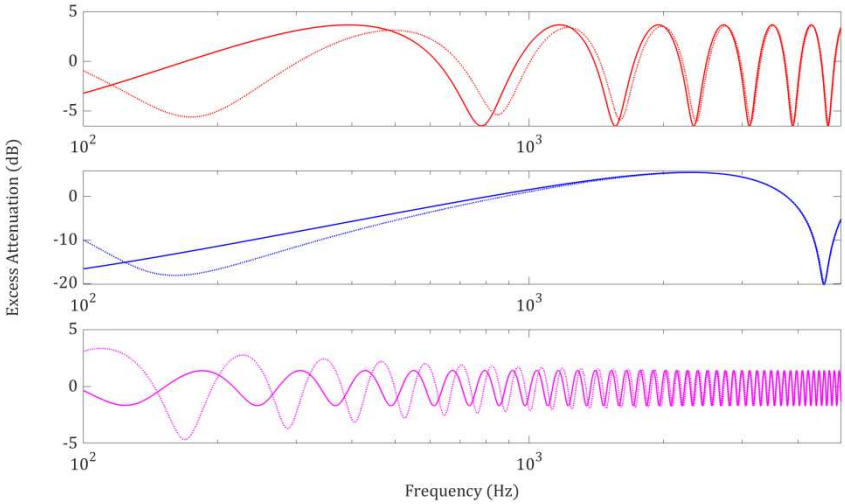

Figure 2: Example excess attenuation spectrum. Top – source/receiver separation is 10m and source/receiver heights are 1.5m. Middle – source/receiver separation is 60m and source/receiver heights are 1.5m. Bottom – source/receiver separation is 10m and source/receiver heights are 4m. Solid line – acoustically 'hard' impedance ground. Dashed line – acoustically 'soft' impedance ground.

excess attenuation spectra over different source/receiver geometries and impedance grounds are illustrated Figure 2. Excess attenuation exhibits oscillatory behaviour as frequency increases and is greatly dependent on the geometrical parameters. However, in real cases the maximum value never exceeds 6dB. The difference in excess attenuation due to the acoustic hardness of the ground is both sensitive to the sound frequency and geometrical parameters. Direct analysis of the excess attenuation is rather complicated because the maxima and minima in this spectrum depend strongly on the problem geometry and ground properties. This makes it difficult to use the excess attenuation spectrum for the ground parameter inversion, source characterisation or for the inversion of the problem geometry acoustically. A question which this paper poses is: *Can we adopt a statistical measure of sound pressure in the wave propagated above porous ground to quantify its variability due to some level of uncertainty in the problem geometry and ground properties?* This paper attempts to answer this question using the probability density function for the excess attenuation of sound propagation above a porous ground in the presence of uncertainties, discovering from sampling methods.

2.1.2 Measuring Impedance

The normalised impedance, Z, in the spherical wave reflection co-efficient (eq. (4)) can be predicted with an acoustic model if the ground is assumed to be porous. The model used in this work was the one proposed by Dazel, Groby and Horoshenkov et al[7]. This model calculates the acoustic properties of the impedance ground by considering the ground as a porous media with circular pores of non-uniform cross-section. This model assumes that the pore size is log-normally distributed. It requires four non-acoustical parameters to predict the ground impedance: (i) porosity (ϕ) ; (ii) tortuosity (α_∞); (iii) median pore size ($\bar{s}$); and standard deviation in the pore size (σ_s). If the median pore size in the ground is much less than the boundary layer thickness for all the frequencies of interest, then it has been shown that one can assume that $\alpha_\infty \sim 1$, $\phi \sim 1$ and $\sigma_s \sim 0$. In this case the only influential parameter is the median pore size, ($\bar{s}$).

In this work we use the Padé approximations for the frequency dependent bulk dynamic density, $\tilde{\rho}(\omega)$, and bulk complex compressibility, $\tilde{C}(\omega)$, in the equivalent fluid model to predict the acoustical properties of porous media with log normal distribution, with circular frequency ω. The bulk dynamic density can be approximated by

$$\frac{\tilde{\rho}(\omega(\epsilon_\rho)}{\rho_0} \simeq \frac{\alpha_\infty}{\phi}\left(1 + \epsilon_\rho^{-2}\tilde{F}_\rho(\epsilon_p)\right), \#(\mathbf{11})$$

where

$$\tilde{F}_\rho(\omega) = \frac{1 + \theta_{\rho,3}\epsilon_\rho + \theta_{\rho,1}\epsilon_\rho}{1 + \theta_{\rho,3}\epsilon_\rho}, \#(\mathbf{12})$$

is the Padé approximation to the viscosity correction function with $\epsilon_\rho = \sqrt{-\frac{i\omega\rho_0\alpha_\infty}{\phi\sigma_g}}$. In these approximations, the coefficients are real and positive numbers with $\theta_{\rho,1} = \frac{1}{3}$, $\theta_{\rho,2} = \sqrt{1/2}e^{\frac{1}{2}(\sigma_s \log(2))^2}$ and $\theta_{\rho,3} = \frac{\theta_{\rho,1}}{\theta_{\rho,2}}$. The equation for the bulk flow resistivity in the porous medium is

$$\sigma_g = \frac{\eta}{\kappa_0} = \frac{8\eta\alpha_\infty}{\bar{s}^2\phi} \mathrm{e}^{6(\sigma_s \log(2))^2}, \#(\mathbf{13})$$

with η being the dynamic viscosity of air and ρ_0 the ambient density of air. Likewise, the bulk complex compresibitly of the fluid in the material pores can be equated as

$$\tilde{C}(\omega) = \frac{1}{\gamma P_0}\left(\gamma - \frac{\gamma - 1}{1 + \epsilon_c^{-2}\tilde{F}_c(\epsilon_c)}\right), \#(\mathbf{14})$$

with

$$\tilde{F}_c(\epsilon_c) = \frac{1 + \theta_{c,3}\epsilon_c + \theta_{c,1}\epsilon_c}{1 + \theta_{c,3}\epsilon_c}. \#(\mathbf{15})$$

In the above two equations $\theta_{c,1} = \frac{1}{3}$, $\theta_{c,2} = \sqrt{\frac{1}{2}}e^{\frac{3}{2}(\sigma_s \log(2))^2}$, $\theta_{c,3} = \frac{\theta_{c,1}}{\theta_{c,2}}$. The frequency dependant parameter is $\epsilon_c = \sqrt{\left(-\frac{i\omega\rho_0 N_{pr}}{\sigma_g'}\right)}$ with γ the ratio of specific heats, N_{Pr} the Pradntl number and P_0 the ambient atmospheric pressure. Thermal flow resistivity is defined here as the inverse of the thermal permeability

$$\sigma_g' = \frac{\eta}{\kappa_0'} = \frac{8\eta\alpha_\infty}{\bar{s}^2\phi} \mathrm{e}^{-6(\sigma_s \log(2))^2} \#(\mathbf{16})$$

Combining eq. (11) and eq. (14) predicts the characteristic acoustic impedance

$$z_b(\omega) = \sqrt{\frac{\tilde{\rho}_b(\omega)}{\tilde{C}_b(\omega)}}, \#(\mathbf{17})$$

and complex wavenumber

$$k_b(\omega) = \omega\sqrt{\tilde{\rho}_b(\omega)C_b(\omega)}, \#(\mathbf{18})$$

in a porous medium with log-normal pore size distribution.

2.2 Simulation Methods

2.2.1 Parameter Uncertainties

To create uncertainty in our desired parameters, random distributions around some true value of interest are generated. The context of true (known) value is that the user may know the true value, whereas our computational model only sees a random number generated from the distribution that was created from the known value. The uncertainty is varied by manipulating the widths of the distributions in proportion to the true value.

Uniform distributions are used to denote uncertainty around a parameter. The uniform distribution denoted U[a,b], is a flat, or *square,* distribution between a lower and upper limit, being a and b here respectively. It is common practice to use uniform and *normal* distributions to simulate error. However, this paper is investigating the systemic uncertainty in the modelling process. Therefore, a flat uncertainty distribution for an input parameter is used so that any parameter value between the bounds is assumed as equally probable. This form of uncertainty is analogous to an observer knowing bounds of a parameter but no other knowledge. It should be

noted that the distribution is *non-normal* by nature. The probability density function (PDF hereon) of the continuous uniform distribution is written as

$$f(x) = \begin{cases} \frac{1}{b-a} & \text{for } a \leq x \leq b, \\ 0 & \text{for } x < a \text{ or } x > b. \end{cases} \#(\mathbf{19})$$

In this study, distributions around some parameter, say y, with the true known true value, y^*, are generated via

$$y \sim U\big((0.95 \times y^*),(1.05 \times y^*)\big), \#(\mathbf{20})$$

$$y \sim U\big((0.8 \times y^*),(1.2 \times y^*)\big). \#(\mathbf{21})$$

$$y \sim U\big((0.65 \times y^*),(1.35 \times y^*)\big). \#(\mathbf{22})$$

This creates a *proportional* uncertainty of $\pm 5\%$, $\pm 20\%$ and $\pm 35\%$ around the true value, respectively. These percentages are chosen to simulate a gradual decrease in the precision of an estimate by an observer, i.e. 5% shows confidence in the chosen interval whereas 35% shows a lack of thorough belief, allowing the value to be within a larger probability distribution interval. Due to the adopted nature of uniform probability distribution our true value is always the mean value as $\mu = \frac{1}{2}(a+b)$. These distributions are applied to simulate uncertainty in source/receiver height and range.

2.2.2 Sampling Methods

The propagation of uncertainty, along with its related effects, is analysed using a basic Monte Carlo method. This simple Monte Carlo method generates a probability density function, or PDF, by repeatedly *sampling* from the parameter distributions described in the previous section and then inputs the generated parameter values, along with known parameters, into the excess attenuation model (eq. (10)) over $10{,}000$ runs. Within the context of uncertainty, it assumed that our model for this purpose of use is *perfect*. Therefore, no error term is included as it is assumed that the model output is precisely the real-life answer produced by the input parameters given.

The frequency range of $100\text{Hz} - 5\text{kHz}$ is used. In this simulation, 1000 frequency points are used, with each point used for the $10{,}000$ main runs to cover equidistantly this broadband frequency range. The frequency range of 100 Hz – 5 kHz was adopted as a balance between computation costs, ability to measure outdoor sound pressures accurately and frequency composition of the sound pressure spectra radiated by realistic sources (see Figures 1.2, 1.3 and 9.25 in ref. [3] and Figure 3.12 in ref. [6]). The choice of frequency range can be important and needs to fit a given application. Appendix A presents data from Monte Carlo simulation showing the effect of the adopted frequency range on the statistical distribution of the access attenuation against an expanded frequency range.

In order to understand better the ground effect on the uncertainty four types of ground are studied: soft (35 kPa m^{-2}); medium (500 kPam^{-2}); hard (2000 kPam^{-2}) and effectively rigid ($20{,}000$ kPam^{-2}). The adopted values of the flow resistivity represent experimental data of real-life impedance grounds[8]: urban grass, sports field, gravel and concrete respectively. It is convenient to adopt a dimensionless parameter when dealing with the problem geometry. An obvious dimensionless parameter is the logarithm of the ratio of source/receiver height over range

$$\Phi = \log_{10}\left(\frac{R_h}{R}\right). \#(\mathbf{23})$$

This parameter controls the problem geometry and its values are listed in Table 1 for a range of source/receiver height and range combinations. The maximum true value of height is 4m due to knowledge that our model would not be as reliable for higher source/receiver positions because of the progressive effect of the wind and temperature gradients. The source height takes the same true value as the receiver height in these simulations for simplicity.

Height (m)	**Range (m)**	**Φ**

1	200	-2.301
1	100	-2
2	100	-1.699
3	100	-1.523
4	100	-1.398
2	25	-1.097
3	25	-0.921
2	9.5	-0.677
3	8.3	-0.442
4	6.6	-0.218
2	2	0

Table 1: Values of Φ and their geometrical parameter combinations.

2.2.3 Statistical Analyses

Statistical analysis accompanies the results from the Monte Carlo simulations. Visually, simulation results are displayed via histograms which present the probability density of the excess attenuation for a given uncertainty in the input parameters. Histograms are generated from the sample data by grouping the data into a number of *bins*. Since bin width is important, Scott's method[9] is used to choose a *sensible* number of bins to be generated from each sample. This method assigns bins based on the sample standard deviation and sample size. This became more important when filtering into octave bands as each band's sample size is different due to the sliding octave band width which increases with frequency.

Statistical moments calculated from the simulated data for the excess attenuation accompany our analysis. Four key moments in this analysis are: mean (μ); standard deviation (σ); skew (s); and kurtosis (k_s) while the mode (M_o) and median (M_{dn}) averages are also investigated. These moments allow us to quantify the behaviour of the probability density function for the excess attenuation presented in the histograms. One behaviour that can be described as *normality*. Normality is a key check with the validity of many statistical tests dependent on this assumption. It has been reviewed that around half of scientific literature articles published contain at least one error, highlighting the need for more validation in future works[10]. Such statistical procedures, especially those commonly used by non-statistical acousticians, such as; correlation, regression, analysis of variance and other such parametric tests are bead on the assumption that the data is normally distributed, or more specifically, that the population that has been sampled from is a normal distribution[11].

Normality can be tested using various methods and tests, but the *Anderson-Darling test (A-D test)* will be used on simulated samples[12]. This test confirms whether the sample came from a population of a given distribution i.e. the normal distribution. It is a modification of *Kolmogrov-Smirnov test*, but gives more weight to the tails. The A-D test makes use of the specific distribution in calculating critical values. The A-D test statistics, A, is defined as

$$A^2 = -N - S \quad \#(\mathbf{24})$$

where

$$S = \sum_{i=1}^{N} \frac{(2i-1)}{N} \left[\ln F(Y_i) + \ln\left(1 = F(Y_{N+1-i})\right)\right] \quad \#(\mathbf{25})$$

N is the sample size, F is the cumulative distribution function (CDF) of the specified parameter distribution (the normal distribution in our case), and Y_i are ordered from smallest to largest. A^2 is then compared to the known *critical value* (C_v) for a given distribution, or the normal distribution for this papers purpose (calculation of this value is outside the scope of this paper). If $A^2 < C_v$ then the null hypothesis (H_0) is accepted, and the data is assumed to follow a normal distribution (normality is not violated). If $A^2 > C_v$, then the null hypothesis is rejected and the alternative hypothesis (H_a) is accepted at a given significance level $(\alpha \leq 0.005)$, allowing us to state the sample does not follow the normal distribution and normality is violated.

The values of the statistical moments are calculated from the simulated broadband and octave band excess attenuation data to be analysed. The median is defined as the middle point value of the data. The mean, or expected value $\mathrm{E}(y) = \mu$, of the data is calculated by

$$\mu = \frac{1}{N}\sum_{i=1}^{N} y_i \,, \#(\mathbf{26})$$

where y_i is a data point in the access attenuation spectrum and N is the total number of data points. These two averages usually are in a similar position in a symmetric distribution. The sample standard deviation, a measure of how much data varies from the mean, is calculated as

$$\sigma = \sqrt{\frac{1}{N-1}\sum_{i=1}^{N}(y_i - \mu)^2} \,. \#(\mathbf{27})$$

The skewness is a measure of asymmetry of data around the sample mean. For example, a perfect uniform distribution would have the value of 0, as would any other perfectly symmetric distribution such as the normal distribution. Negative and positive of skewness mean that the sample data is *stretched* more to the left or right from the mean, respectively. As general rule, data which has skewness of less than $|\pm 0.5|$ can be considered symmetrical. Data is highly skewed when skewness exceeds $|\pm 1|$. If the skewness is larger than 2, or smaller than -2, then the data is strongly non-normal[12]. The skewness is calculated as

$$s = \frac{\sum_{\mathrm{i}=1}^{\mathrm{N}}(y-\mu)^3/N}{\sigma^3} \,. \#(\mathbf{28})$$

Kurtosis measures how outlier prone, or how heavy-tailed or light-tailed the distribution is, in relation to a normal distribution. The kurtosis of perfect normal distribution is 3, while the kurtosis of a perfect uniform distribution is 1.8. Distributions that are more, or less outlier-prone than the perfect normal distribution have kurtosis greater, or less, than 3 respectfully. Kurtosis values between 1 and 5 are accepted for the assumption of normality[12], while vales below 0 or greater than 7 would indicate a substantial departure from normality[12]. This final value is equated as

$$k_s = \frac{\sum_{\mathrm{i}=1}^{\mathrm{N}}(y-\mu)^4/N}{\sigma^4} \,. \#(\mathbf{29})$$

The median (M_{dn}) is found by locating the $\left(\frac{\mathrm{n}}{2}\right)^{\mathrm{th}}$ point in the data set, where n is the number of points in the set. Since our data samples are an even numbered, the *middle value* between the two numbers that surround the $\left(\frac{\mathrm{n}}{2}\right)^{\mathrm{th}}$ point is taken. The mode (M_o) is taken as the estimate that appears the most, also seen as the most likely value in the PDF (Figures 3-6)

3 Results

The effect of ground impedance is well known to be greatly influential on the acoustical signal. However, the differences in the PDFs for the excess attenuation found for different values of Φ over the different ground types are not as pronounced as expected (see Figures (3-6)). Sample means and medians did not significantly differ across the range of the flow resistivity, σ_g. However, some statistical moments do show some consistent differences. This strongly suggests that the effect of the problem geometry on the excess attenuation statistics are dominant for this particular propagation model

3.1 Exploring Φ and σ_g

Some differences do exist in the simulated PDFs for the different values of flow resistivity σ_g (see Figures 3-6) and there these behaviours are mirrored in the value of the statistical moments (see Table 2 and 3). However, there is some consistency in the PDF for particular values of the parameter Φ. The most obvious differences between the results for different impedance grounds are for $\Phi < -2$. As σ_g is increased, the long smooth distribution has its deviation reduced by half between the softest and hardest impedance grounds (see Figure 3 and 6 respectively). It is unclear what distribution these results follow. The PDFs presented in Figure 3-6 appearing irregular and suggest some non-normality within the data.

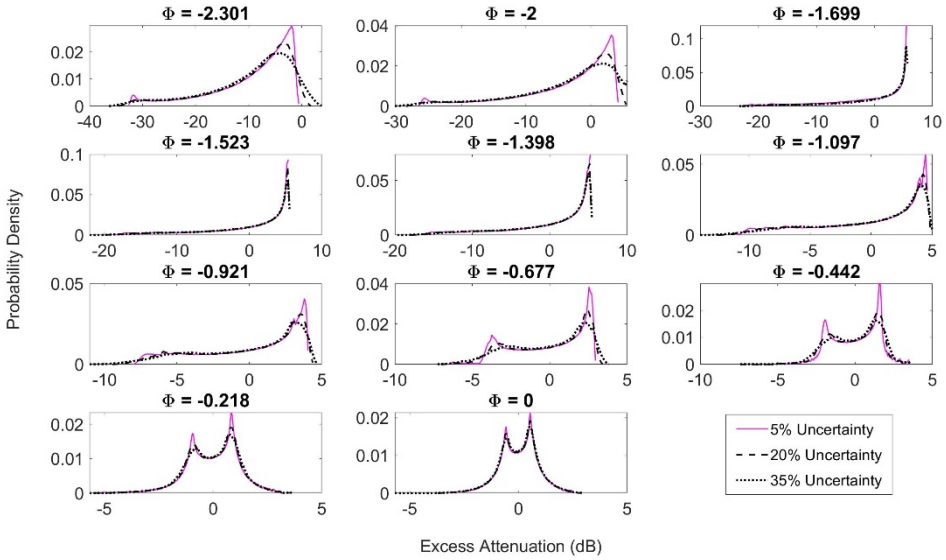

Figure 3: The PDFs of excess attenuation spectra for a range of values of Φ and levels of uncertainties in the source/receiver coordinates. The flow resistivity of the ground is $\sigma_g = 35\text{kPasm}^{-2}$.

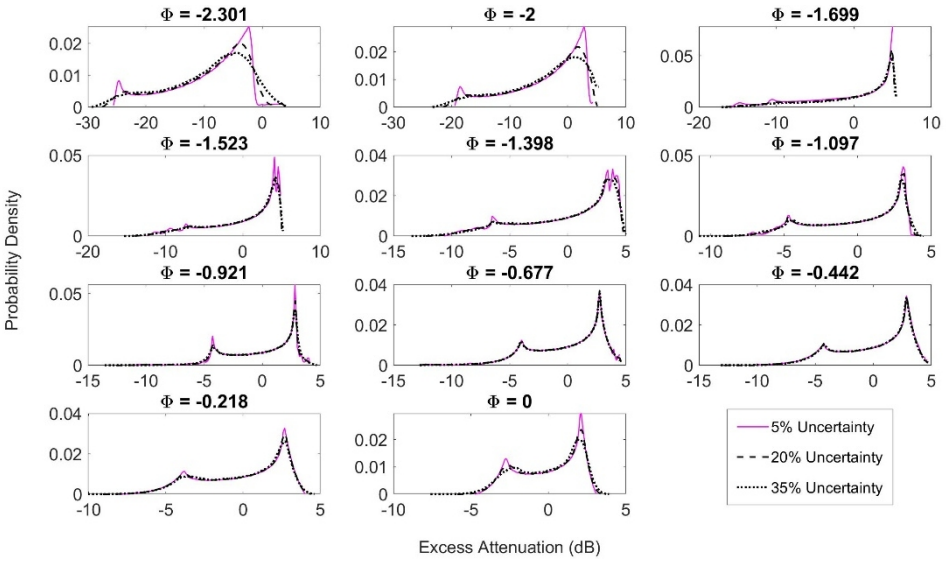

Figure 4: The PDFs of excess attenuation spectra for a range of values of Φ and levels of uncertainties in the source/receiver coordinates. The flow resistivity of the ground is $\sigma_g = 500\text{kPasm}^{-2}$.

When $-2 < \Phi < -1$ the PDF for the excess attenuation contains a clear peak which amplitude depends on the level of uncertainty in the adopted values of geometrical parameters. These data are associated with a strongly negative skewness and relatively large standard deviation (see Table 3). These peaks appear in the range of 0dB

$< \Delta L <$ 5dB. A very small secondary peak emerges at $\Delta L \approx -$ 5dB, doing so more strongly as σ_g increases. The second peak in the PDF becomes clearly visible in the range of $\Delta L \leq -$ 5dB when the ratio Φ increases for $\Delta L > -$ 1. The peaks initial value changes depending on the value of σ_g, yet with no consistent pattern in relation to the change of σ_g. This peak directly relates to the mode (see Table 2), which makes the behaviour easier to describe. The amplitude of this second negative peak increases with an increase in the ratio Φ with its position moving progressively towards $\Delta L = -$ 1dB for the lowest value of σ_g and to $\Delta L = -$ 4dB for the highest value of σ_g.

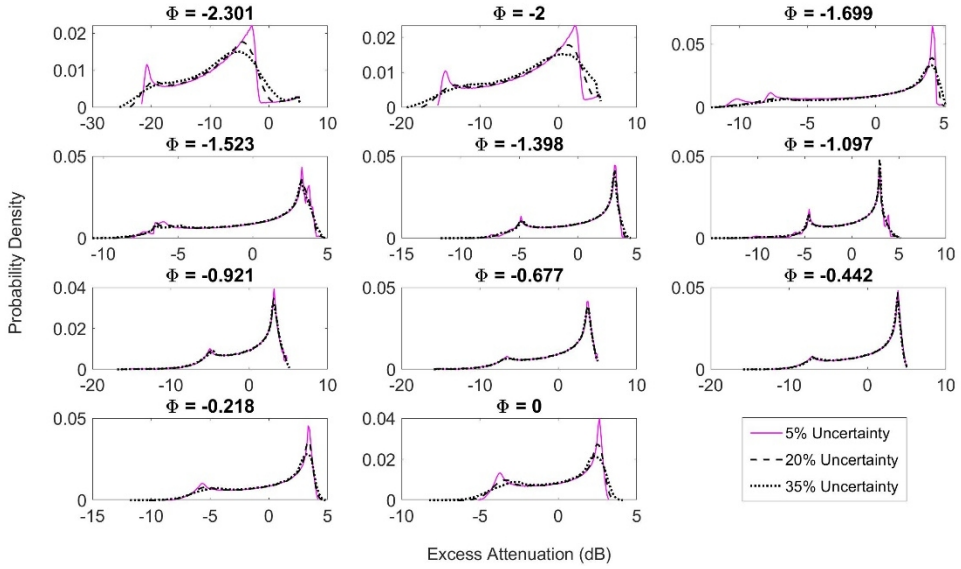

Figure 5: The PDFs of excess attenuation spectra for a range of values of Φ and levels of uncertainties in the source/receiver coordinates. The flow resistivity of the ground is $\sigma_g = 2000\text{kPasm}^{-2}$.

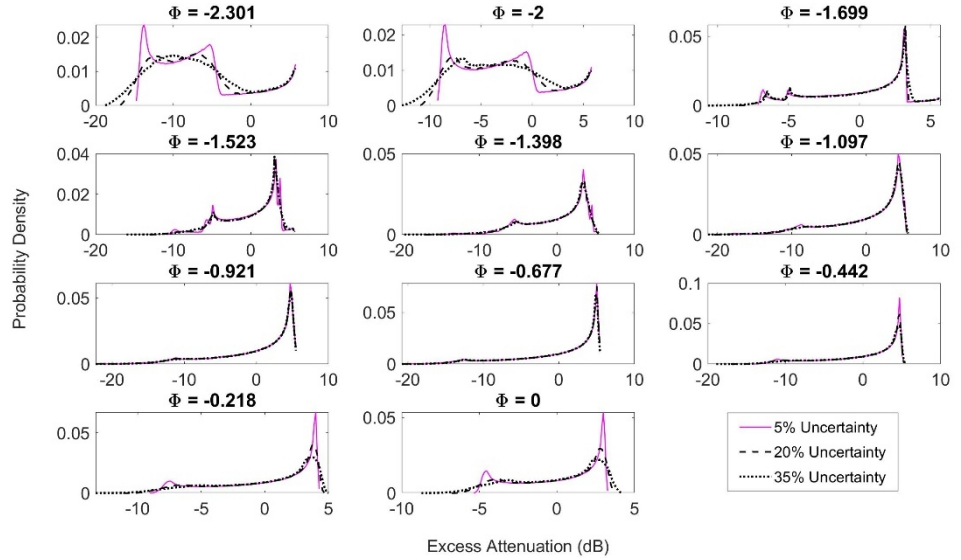

Figure 6: The PDFs of excess attenuation spectrum for a range of values of Φ and levels of uncertainties in the source/receiver coordinates. The flow resistivity of the ground is $\sigma_g = 20{,}000\text{kPasm}^{-2}$.

For ratios $\Phi \approx 0$ the PDF of the excess attenuation spectrum appears increasingly bimodal, with the space between peaks increased, and the strength of the negative peak decreased, by the increase in σ_g. However, the increase in uncertainty and σ_g negates the second peak at the negative point, smoothing out the distribution.

3.2 Simulation statistics

The statistics can be described by a number of *statistical moments*. It seems that the statistics for $\Phi <- 2$ are inconsistent, and hard to describe in relation to combinations of differing values for Φ, σ_g and uncertainty.

Looking at the averages, the mean (see the 3rd column of Table 2) is the most stable and unaffected. For $\Phi >- 1$, the mean is close to 0dB. For $\Phi <- 2$ the mean is highly negative (see Table 2). This behaviour is seemingly unaffected by the change in the uncertainty level. As the ground becomes much harder, the mean for $\Phi <- 2$ increases.

σ_g	Φ	Mean (μ)			Mode (M_o)			Median (M_{dn})		
	-2.301	-9.462	-9.469	-9.482	-1.905	-3.17	-4.099	-6.997	-7.109	-7.367
	-2	-3.818	-3.844	-3.905	3.187	2.039	1.889	-1.304	-1.410	-1.654
	-1.699	-1.074	-0.387	0.065	5.524	5.614	5.455	1.413	2.188	2.679
	-1.523	0.217	-0.014	0.028	5.392	5.287	5.344	2.673	2.376	2.407
	-1.398	0.108	0.017	0.026	5.068	5.167	5.068	2.322	2.207	2.192
35kPasm^{-2}	-1.097	0.007	-0.059	-0.048	4.461	4.241	4.114	1.600	1.497	1.481
	-0.921	-0.038	-0.045	-0.035	3.807	3.516	2.929	1.078	1.059	1.042
	-0.677	-0.055	-0.055	-0.054	2.536	2.419	2.305	0.508	0.504	0.489
	-0.422	0.021	0.019	0.012	1.562	1.48	1.302	0.252	0.250	0.247
	-0.218	-0.007	-0.006	-0.002	0.84	0.808	0.802	0.105	0.108	0.109
	0	0.013	0.012	0.009	0.54	0.547	0.511	0.068	0.065	0.064
	-2.301	-9.327	-9.332	-9.343	-2.283	-3.804	-5.079	-7.381	-7.490	-7.739
	-2	-3.839	-3.864	-3.924	2.785	1.51	1.165	-1.866	-1.965	-2.198
	-1.699	-1.025	-0.395	-0.007	4.996	4.876	4.897	0.814	1.505	1.954
	-1.523	0.038	-0.119	-0.078	4.089	4.246	4.246	1.664	1.446	1.475
	-1.398	-0.033	-0.089	-0.079	3.869	4.087	3.598	1.277	1.197	1.199
500kPasm^{-2}	-1.097	-0.095	-0.104	-0.097	3.094	3.156	2.975	0.748	0.744	0.758
	-0.921	-0.088	-0.092	-0.091	2.816	2.861	2.781	0.655	0.647	0.668
	-0.677	-0.089	-0.086	-0.083	2.767	2.741	2.773	0.746	0.753	0.762
	-0.422	0.023	0.014	0.009	2.86	2.917	2.862	0.932	0.924	0.904
	-0.218	-0.01	-0.006	-0.003	2.694	2.694	2.694	0.709	0.707	0.696
	0	0.012	0.011	0.01	2.122	2.129	1.925	0.672	0.677	0.689
	-2.301	-8.884	-8.888	-8.894	-2.867	-4.481	-5.256	-7.623	-7.726	-7.96
	-2	-3.698	-3.723	-3.78	2.078	1.331	0.427	-2.333	-2.427	-2.636
	-1.699	-0.794	-0.294	0.004	4.153	4.148	4.112	0.566	1.063	1.434
	-1.523	-0.059	-0.128	-0.095	3.285	3.255	3.25	1.02	0.924	0.966
	-1.398	-0.087	-0.105	-0.097	3.113	3.146	3.07	0.806	0.793	0.809
2000kPasm^{-2}	-1.097	-0.151	-0.111	-0.109	3.007	2.943	3.016	0.715	0.801	0.825
	-0.921	-0.097	-0.098	-0.101	3.179	3.113	3.074	1.016	1.015	1.012
	-0.677	-0.097	-0.091	-0.088	3.804	3.683	3.855	1.333	1.331	1.319
	-0.422	0.022	0.012	0.007	3.895	3.878	3.788	1.445	1.422	1.396
	-0.218	-0.011	-0.006	-0.003	3.36	3.398	3.331	1.028	1.021	1.007
	0	0.016	0.009	0.007	2.625	2.508	2.331	0.599	0.586	0.585
	-2.301	-6.874	-6.870	-6.855	-13.779	-6.649	-9.912	-7.677	-7.746	-7.756
	-2	-2.941	-2.959	-2.993	-8.509	-7.561	-6.769	-3.131	-3.199	-3.296
	-1.699	-0.019	0.002	0.037	3.129	3.246	3.198	0.87	0.951	1.048
	-1.523	-0.26	-0.123	-0.123	3.266	3.054	3.05	0.629	0.92	0.947
	-1.398	-0.178	-0.114	-0.117	3.403	3.418	3.215	1.032	1.151	1.158
20000kPasm^{-2}	-1.097	-0.208	-0.114	-0.124	4.305	4.301	4.39	1.611	1.746	1.731
	-0.921	-0.103	-0.097	-0.106	4.691	4.717	4.732	1.990	1.992	1.972
	-0.677	-0.102	-0.092	-0.093	4.995	5.02	4.844	2.076	2.076	2.061
	-0.422	0.02	0.009	0.006	4.713	4.743	4.705	1.937	1.913	1.886
	-0.218	-0.011	-0.006	-0.003	4.011	3.87	3.654	1.311	1.304	1.287
	0	0.016	0.008	0.006	2.994	2.728	2.51	0.741	0.729	0.73

Table 2: Collated sample averages from simulations for each combination of σ_g and Φ. Columns from left to right are for uncertainties from 5%, 20% and 35%, respectively.

This suggests that the true mean of the population (the data set which each sample intends to replicate) is not strongly affected by the variation in Φ or σ_g. This is useful for shaping fitting distribution to data that require the use of the mean i.e. the normal distribution of $N \sim (\mu, \sigma^2)$.

The median (see the 4th column of Table 2) follows a similar behaviour to that observed for the mean while around ~ 1dB higher. For a harder ground ($\sigma_g \geq 2000\text{kPasm}^{-2}$) it displays an oscillatory behaviour as a function of Φ. The increased median, in relation to the respective mean for a given Φ and σ_g is expected due to the negative skew.

The most repeated observed value, the mode (M_o) (see the last column of Table 2), is the average most effected by σ_g, Φ and uncertainty. The mode begins at $\sim$5dB when $\phi \approx -2$ which decreases to $\sim$2dB when Φ is decreased to zero. Each mode is reduced by $\sim$0.5dB per each increase in σ_g at every respective related value of Φ. Uncertainty does increase the mode for higher values of σ_g, with little difference seen between mode for the softest impedance ground. Modes when $\phi < -2$ show the greatest difference, with the lowest σ_g giving values between approximately $-5 < M_0 < 3$ while at the hardest impedance ground, the range of mode is halved and decreased to around $-13 < M_o < -7$. The increase from the median and mean was again an expected side effect of the negative skewness present in the samples. In the case of symmetric distributions, the mode quite often relates to parameter estimation techniques, highlighting the need for quantifying Φ and σ_g efficiently.

The second grouping of statistics (Table 3) are the higher moments such as the standard deviation (σ), skewness (s) and kurtosis (k_s). Behaviours for the increase/decrease in the varying control parameters ϕ, σ_g and uncertainty are clearer for these statistical moments than the earlier averages (Table 2).

σ_g	Φ	Std. Dev (σ)			Skewness (s)			Kurtosis (k_s)		
	-2.301	7.661	7.768	8.011	-1.226	-1.171	-1.058	3.777	3.714	3.578
	-2	7.384	7.464	7.64	-1.284	-1.245	-1.17	3.92	3.873	3.77
	-1.699	6.987	6.649	6.431	-1.134	-1.318	-1.428	3.365	3.893	4.253
	-1.523	5.94	5.998	5.959	-1.332	-1.276	-1.291	3.85	3.705	3.786
	-1.398	5.54	5.564	5.537	-1.193	-1.172	-1.186	3.399	3.365	3.456
35kPasm^{-2}	-1.097	4.369	4.381	4.362	-0.84	-0.83	-0.859	2.456	2.474	2.616
	-0.921	3.51	3.512	3.51	-0.643	-0.658	-0.701	2.077	2.154	2.341
	-0.677	2.368	2.381	2.412	-0.452	-0.472	-0.511	1.87	1.963	2.143
	-0.422	1.539	1.559	1.596	-0.322	-0.35	-0.402	2.267	2.342	2.516
	-0.218	1.192	1.196	1.203	-0.485	-0.469	-0.441	3.644	3.644	3.571
	0	0.884	0.89	0.904	-0.263	-0.269	-0.306	3.369	3.469	3.71
	-2.301	6.778	6.891	7.151	-0.792	-0.749	-0.664	2.631	2.633	2.623
	-2	6.322	6.409	6.604	-0.878	-0.849	-0.794	2.679	2.699	2.719
	-1.699	5.724	5.381	5.216	-0.807	-0.963	-1.043	2.503	2.86	3.056
	-1.523	4.502	4.532	4.506	-0.891	-0.874	-0.896	2.632	2.646	2.747
	-1.398	3.955	3.974	3.971	-0.76	-0.757	-0.783	2.373	2.401	2.519
500kPasm^{-2}	-1.097	3	3.022	3.057	-0.57	-0.576	-0.603	2.02	2.056	2.156
	-0.921	2.83	2.85	2.889	-0.715	-0.711	-0.71	2.829	2.816	2.8
	-0.677	3.123	3.123	3.119	-0.805	-0.801	-0.795	3.131	3.099	3.051
	-0.422	3.166	3.163	3.138	-0.662	-0.679	-0.69	2.367	2.445	2.519
	-0.218	2.738	2.734	2.725	-0.535	-0.546	-0.562	2.039	2.096	2.193
	0	1.988	2.006	2.045	-0.378	-0.391	-0.43	1.789	1.869	2.05
	-2.301	6.18	6.296	6.559	-0.331	-0.317	-0.292	2.368	2.375	2.378
	-2	5.426	5.521	5.731	-0.57	-0.554	-0.529	2.164	2.22	2.305
	-1.699	4.601	4.303	4.219	-0.593	-0.713	-0.787	2.025	2.266	2.421
	-1.523	3.477	3.497	3.512	-0.616	-0.614	-0.646	2.036	2.073	2.178
	-1.398	3.096	3.121	3.159	-0.589	-0.593	-0.62	2.044	2.075	2.177
2000kPasm^{-2}	-1.097	3.217	3.235	3.279	-0.763	-0.791	-0.794	2.853	2.913	2.934
	-0.921	3.663	3.674	3.689	-0.906	-0.906	-0.903	3.285	3.278	3.259
	-0.677	4.229	4.213	4.18	-0.906	-0.905	-0.898	2.927	2.925	2.9
	-0.422	4.077	4.069	4.036	-0.805	-0.814	-0.821	2.437	2.488	2.546
	-0.218	3.339	3.339	3.34	-0.62	-0.636	-0.665	2.039	2.111	2.247
	0	2.358	2.383	2.436	-0.433	-0.451	-0.499	1.767	1.858	2.06
	-2.301	5.636	5.732	5.94	0.715	0.639	0.49	2.591	2.523	2.399
	-2	4.144	4.231	4.416	0.392	0.338	0.229	2.231	2.196	2.143
	-1.699	3.311	3.354	3.423	-0.532	-0.554	-0.596	2.158	2.165	2.227
	-1.523	3.564	3.588	3.642	-0.692	-0.779	-0.799	2.63	2.77	2.866
	-1.398	3.958	3.967	4.007	-0.896	-0.94	-0.955	3.116	3.224	3.302
20000kPasm^{-2}	-1.097	5.068	5.049	5.062	-1.055	-1.098	-1.104	3.29	3.398	3.429
	-0.921	5.488	5.481	5.464	-1.171	-1.172	-1.164	3.535	3.539	3.515
	-0.677	5.642	5.615	5.571	-1.158	-1.155	-1.146	3.354	3.351	3.33
	-0.422	4.987	4.983	4.957	-0.993	-1.005	-1.022	2.798	2.861	2.968
	-0.218	3.864	3.872	3.89	-0.716	-0.74	-0.789	2.164	2.27	2.481
	0	2.663	2.694	2.76	-0.487	-0.509	-0.568	1.806	1.914	2.153

Table 3: Collated sample statistical moments from simulations for each combination of σ_g and Φ. Columns from left to right are for uncertainties from 5%, 20% and 35%, respectively.

The standard deviation is most effected by the value of σ_g and Φ (3rd column of Table 3). The standard deviation for the minimum value of $\Phi = -2.301$ has the maximum. As $\Phi \rightarrow 0$ the value of the standard deviation reduces consistently for all ground types. The standard deviation generally reduces with the increase in the value of σ_g for $\Phi < -1$. For $\Phi \approx 0$ the standard deviation slightly increases with the increased flow resistivity of the ground. The effect of the geometrical uncertainty on the standard deviation is relatively small.

The skewness (4th column of Table 3) is seen to be consistently negative but increasing with the increasing value of Φ in the case of the softest ground ($\sigma_g = 35$ kPasm^{-2}). As the value of σ_g increases to 20,000 kPasm^{-}

[2] this dependence changes and the skewness seems to have a clear minimum for $-1 < \Phi < 0.5$. For the flow resistivity values between these extreme ground cases the skewness behaves as an oscillatory function of Φ. The geometrical uncertainty does not affect this parameter significantly for $\Phi > -1.5$.
The behaviour of the kurtosis as a function of Φ (5th column of Table 3) shows a clear minimum around $-1 < \Phi < -1.5$ for the case with the softest ground. For the hardest ground this minimum becomes the maximum. For the cases with $35 < \sigma_g < 2000$ kPasm^{-2} this behaviour is complex and oscillatory. The geometrical uncertainty does not affect this parameter significantly.

3.3 Normality Assumption

Normality is an assumption that needs to be taken seriously. When this assumption is violated, it becomes harder to draw accurate and reliable statistical conclusions[14]. In the case of higher-order statistical moments (Table 3) there is no visual indication that normality has been violated. However, the non-normal indicators are checked through the Anderson-Darling test which is applied to the simulation data from each combination of Φ, σ_g and uncertainty level. It is found that every single sample significantly $(p \ll 0.005)$ rejected the null hyposthesis that the sample was normal. This indicates that it is the data obtained violate the normality assumption.

This could indicate one of the following scenarios: (i) a certain combination of the frequency range over which the data are analysed, Φ and/or uncertainty create non-normal PDFs; (ii) the initial *prior* uniform distribution propagates through its non-normality; (iii) the acoustic prediction model is non-normal in itself. It is not of ease to state which the causes is nor is it any easier to prove. More investigation into the physics underpinning the interactions between Φ, σ_g and acoustic wavelength, λ is required. It is also useful to investigate how great an effect the distribution of the uncertainty in unknown parameters is. This could be can be done be comparing simulation results from known prior distributions and using statistical test to investigate whether the final sample changes accordingly, yet this work lies outside the main scope of this work.

4 Conclusions

The effect of the impedance grounds on the statistics in the excess attenuation data was significantly related to the test statistic chosen. The mean and median values of the excess attenuation did not change significantly (within 1/100th of a dB) as the ground properties have changed from soft to hard. However, the mode and later statistical moments did differ in relation to the values of σ_g. The mode and standard deviation were most significantly affected by the change in σ_g. The deviation decreasws in parallel with the increase of σ_g while the modes oscillatory behaviour around Φ had the range between the maximum and minimum modes decrease with the increase in σ_g. It is known that varying ground can make a very strong effect on the excess attenuation spectrum, but this shows a relatively small effect on mean, skewness and kurtosis when the model geometry is uncertain. In contrast, the modes dependence on both Φ and σ_g is crucial as common point estimation inference techniques, such as maximum likelihood methods, are directly linked to this statistic, thus an inaccurate estimation of the mode will hinder effective parameter estimations. These findings highlight the importance of removing such geometric uncertainties before making predictions or using excess attenuation data for parameter inversion. Inference work using more uncertain or complex models could also benefit from these findings, relying on the ability to either select arbitrary impedance values or save computation time drawing from these known PDF while have uncertainties, at minimum, present in the ground and receiver geometry. This would greatly reduce computational costs while having a likely negligible effect on accuracy.

The behaviour of the broadband excess attenuation PDF as a function of Φ is rather informative. When $\Phi < -1$ the PDFs contain a clear peak which amplitude depends on the level of uncertainty in Φ. These data are associated with a strongly negative skewness and relatively large standard deviation. For $\Phi < -2$ the PDF shifts in its entirety across the excess attenuation scale (x-axis) to around ~ -5dB , however has no obvious defined distribution, which is exacerbated across varying σ_g . For the ratio $\Phi \approx -1$ the standard deviation in the data, skewness and kurtosis reduce with a second peak becoming visible in the range of $\Delta L \leq -10$dB. When the ratio Φ increases above -1, the second peak in the PDF at $\Delta L \leq 0$dB becomes very pronounced. The amplitude of this peak increases with the increase in the ratio Φ and its position moves progressively towards $\Delta L = -1$dB, converging the two peaks. The PDFs appear to become *bimodal* in nature due to the strength of this secondary peak. The convergence of the *negative peak* is hindered with both its increase in the related excess attention value (x-axis) and probability clue (y-axis), as well as the convincing appearance of a bimodal distribution, by

the increase in σ_g and uncertainty. Being able to understand and/or control the PDF using this numerical value of Φ, solely and in combination with σ_g, will be of great use for future statistical methods to parameter inversion and may hint towards methodologies to use i.e. regression methods since interactions between parameters are likely to help prior selection while using Bayesian methods. The more pronounced bimodality at lower σ_g may also suggest reasoning to inaccuracies during measurement in low impedances i.e. convergence to wrong peak during calculation of the mean.

Most statistical inference is done via parametric methods i.e. assumes the observe data available follows a normal distribution. However, if normality is found to be violated, then the validity of the results gained using such methods is compromised[10–14]. None of the indicator statistics had values that indicated non-normal behaviour, however the movement of the kurtosis values indicated some of the samples were acting peculiar. The Anderson-Darling tests that were performed were shown to extremely support the assumption that each sample violated normality, with substantial confidence $(p \ll 0.05)$. It is unclear what caused these irregularities: the uniform sampling distribution or physical phenomena from Φ with the frequency bands themselves. Investigating the physics underpinning the interactions between Φ and λ, while comparing the effect of using normal and non-normal distributions to sample will hopefully recover the true reason. This also highlights the need to validate the normality assumption before progressing with statistical processes on a given data set, a process which is majorly overlooked.

Future research would require an investigation into a more complex sound propagation model that allows for meteorological effects. This would reveal how strong the influence of the geometrical uncertainties is in relation to the influence of stochastic meteorological effects and ground effects. It would also reveal the relative *strength* of uncertainty in different input parameters on the excess attenuation. Regression methods on real data sets could also be used to investigate such behaviours as interaction effects etc. The parameter Φ could be used to strengthen the effectiveness of the regression either as an additional parameter or even instead of the receiver parameters. Investigating of the effect of a broader range of values of Φ on the excess attenuation statistics will also be of interest to expand current understanding. This may require a more complicated propagation model which includes a realistic ground topography, effects of buildings and vegetation in the propagation path. Investigation of a dimensionless parameter from a combination of Φ, σ_g and k to shape likelihood distributions would likely be successful. This could also be extended to other models to see if attributes of Φ remain constant. Finally, discovering the cause of the non-normal behaviour in the predicted statistical moments for the excess attenuation is a key to better understanding of the capabilities and limitations in the statistical simulation of sound propagation in the presence of uncertainties. Performing rigorous normality tests for results from differing Φ and σ_g, both for broadband and narrowband samples, will be a step forward to discovering if they are true anomalies or a product of the non-normal input prior. We theorise it is possible that the extreme non-normality is a product of some interference patterns produced by certain values of Φ at relevant frequencies rather than prior parameter distribution being non-normal or normal.

5 Acknowledgements

The author/s acknowledge the support of Defense Science and Technology Laboratory (Dstl) UK and EPSRC CASE studentship award to the University of Sheffield. The authors are also grateful to Prof. Jeremy Oakley from the Department of Mathematics and Statistics at the University of Sheffield for his useful comments on the statistical aspects of this work.

6 References

[1] C. L. Pettit and D. K. Wilson. 'Uncertainty and stochastic computations in outdoor sound propagation', J. Acoust. Soc. Am., 135(4). (May 2014).

[2] C. L. Pettit, D. K. Wislon, V. E. Ostashev and S. N. Vecherin. "Description and quantification of uncertainty in outdoor sound propagation calculations," J. Acoust. Soc. Am., 136(3). (September 2014).

[3] K. Attenborough, K.M. Li and K.V. Horoshenkov. Predicting Outdoor Sound. CRC Press. (2006)

[4] D. C. Hothersall and J. N. B. Harriott. 'Approximate models for sound propagation above multi-impedance plane boundaries', J. Acoust. Soc. Am., 97(2), 918-926. (Feb 1995).

[5] R. Kruse and V. Mellert. 'Effect and minimization of errors in in situ ground impedance measurements', Applied Acoustics, 69(10), 884-890. (October 2008).

[6] E.M. Salomons. Computational Atmospheric Acoustics, Kluwer Academic Publishers, 5-27. (2001).

[7] O. Dazel, J.P. Groby and K.V. Horoshenkov. 'Asymptotic limits of some models for sound propagation in porous media and the assignment of the pore characteristic lengths', J. Acoust. Soc. Am., 139(5), 2463-2474. (May 2016).
[8] K. Attenborough, 'Outdoor ground impedance models', J. Acoust. Soc. Am., 129(50), 2806-2819. (May 2011).
[9] D. W. Scott. 'On Optimal and Data-Based Histograms', Biometrika, 66(3), 605-610. (Decemeber 1979).
[10] Ghasemi, A., & Zahediasl, S. 'Normality tests for statistical analysis: a guide for non-statisticians.' Int. J. Endo. Metab., 10(2), 486. (April 2012)
[11] P. J. Curran, J. F. Finch and S. G. West. 'Structural Equation Modelling: Concepts, Issues, and Applications' in *Structural equation models with non-normal variables: Problems and remedies*, Sage Publications Inc., 56-75. (1995)
[12] A. Field. Discovering Statistics Using SPSS, London: Sage Publications Ltd.. (2009).
[13] M.A. Stephens, 'EDF Statistics for Goodness of Fit and Some ~~Comaprisons~~Comparisons', J. Am. Stats. Asoc., 69(346), 730-737. (September 1974).
[14] A.H. Elhan, D. Otzuna and E. Tuccar. 'Investigation of four different normality tests in terms of type 1 error rate and power under different distributions', Turk. J. Med. Sci., 36(3), 171-176. (January 2006).
[15] "ISO 9613-2:1996." ISO, 12 June 2017, https://www.iso.org/standard/20649.html.
[16] "European Commission." CORDIS, https://cordis.europa.eu/project/rcn/57829/factsheet/en.

7 Appendix A. The effect of frequency range

The choice of frequencies in this paper is based on the fact that a majority of sources of outdoor noise emit efficiently frequencies of sound between 100 Hz and 5 kHz[3,6]. This range is sensible to find a balance between computational costs and accuracy in the statistical data attained from the Monte Carlo simulation.

The frequency ranges suggested in some popular prediction standards may differ from the range adopted in this paper. The ISO 9613 Part 2 standard[15] suggests that the calculations should be carried out in the octave bands between 63 and 8000 Hz. The Harmonoise prediction standard[16] suggests that this range should be between 25 Hz and 20 kHz.

The probability density functions for the excess attenuation presented below illustrate the effect of the spectral width. This difference is between the 100 Hz – 5 kHz range and 25 Hz – 20 kHz range is not large, but noticeable dependent on Φ and σ_g. Therefore, it should be recommended to ensure that the spectrum of the source is properly captured in this type of analysis by adopting the right frequency range.

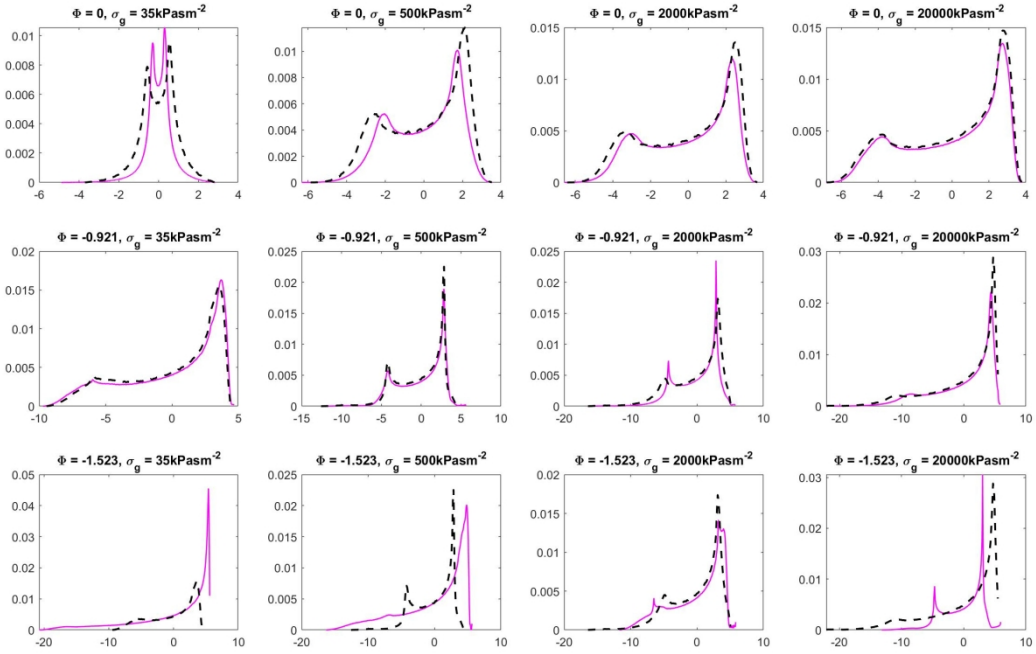

Figure A1: The effect of the choice of the frequency range on the probability density function for the excess attenuation predicted with the adopted Monte Carlo simulation. The uncertainty is 20%. Black dashed line: frequency band 100 Hz – 5 kHz. Magenta: 25 Hz – 20 kHz.

Declaration of interests

 The authors declare that they have no known competing financial interests or personal relationships that could have appeared to influence the work reported in this paper.

☐The authors declare the following financial interests/personal relationships which may be considered as potential competing interests:

Each of the nominated authors has concurred and is in agreement with the content of the paper.

Jordan A. Parry – JAParry1@sheffield.ac.uk

Kirill V. Horoshenkov – K.horoshenkov@sheffield.ac.uk

Duncan P. Williams – DPWilliams@dstl.gov.uk